Allosteric Regulation Provides a Molecular Mechanism for Preferential Utilization of the Fully Assembled Dolichol-Linked Oligosaccharide by the Yeast Oligosaccharyltransferase†

Denise Karaoglu, Daniel J. Kelleher, and Reid Gilmore*

Department of Biochemistry and Molecular Pharmacology, University of Massachusetts Medical School, Worcester, Massachusetts 01655-0103

Received June 8, 2001; Revised Manuscript Received August 9, 2001

ABSTRACT: The oligosaccharyltransferase (OST) preferentially utilizes the fully assembled dolichol-linked oligosaccharide $Glc_3Man_9GlcNAc_2$-PP-Dol as the donor for N-linked glycosylation of asparagine residues in N-X-T/S consensus sites in newly synthesized proteins. A wide variety of assembly intermediates ($Glc_{0-2}Man_{0-9}GlcNAc_2$-PP-Dol) can serve as the donor substrate for N-linked glycosylation of peptide acceptor substrates in vitro or of nascent glycoproteins in mutant cells that are defective in donor substrate assembly. A kinetic mechanism that can account for the selection of the fully assembled donor substrate from a complex mixture of dolichol-linked oligosaccharides (OS-PP-Dol) has not been elucidated. Here, the steady-state kinetic properties of the OST were reinvestigated using a proteoliposome assay system consisting of the purified yeast enzyme, near-homogeneous preparations of a dolichol-linked oligosaccharide ($Glc_3Man_9GlcNAc_2$-PP-Dol or $Man_9GlcNAc_2$-PP-Dol) and an ^{125}I-labeled tripeptide as the acceptor substrate. The K_m of the OST for the acceptor tripeptide was only slightly enhanced when $Glc_3Man_9GlcNAc_2$-PP-Dol was the donor substrate relative to when $Man_9GlcNAc_2$-PP-Dol was the donor substrate. Evaluation of the kinetic data for both donor substrates showed deviations from typical Michaelis−Menten kinetics. Sigmoidal saturation curves, Lineweaver−Burk plots with upward curvature, and apparent Hill coefficients of about 1.4 suggested a substrate activation mechanism involving distinct regulatory (activator) and catalytic binding sites for OS-PP-Dol. Results of competition experiments using either oligosaccharide donor as an alternative substrate were also consistent with this hypothesis. We propose that binding of either donor substrate to the activator site substantially enhances $Glc_3Man_9GlcNAc_2$-PP-Dol occupancy of the enzyme catalytic site via allosteric activation.

In eukaryotic organisms, N-linked glycosylation is an essential protein modification pathway that is initiated within the lumen of the rough endoplasmic reticulum (RER)[1] (for reviews see refs *1* and *2*). The oligosaccharyltransferase (OST, EC 2.4.1.119), catalyzes the formation of a covalent N−C bond between the C-1 position of GlcNAc in a high-mannose oligosaccharide ($G_3M_9GN_2$) and an asparagine residue in the nascent polypeptide. Asparagine acceptor sites for N-linked glycosylation have the consensus sequence N-X-T/S where X can be any amino acid except proline (*3*). The OST will glycosylate synthetic N-X-T/S tripeptides, provided that the two termini are capped by protecting groups mimicking a peptide backbone (*4*). A variety of synthetic peptides differing in length, sequence, and capping groups have been used as substrates to derive Michaelis−Menten steady-state kinetic parameters for the peptide substrate (*5*−*11*). The donor substrate (OS-PP-Dol) for N-linked glycosylation is a preassembled oligosaccharide ($G_3M_9GN_2$) linked to the polyisoprenoid dolichol via a pyrophosphate linkage. Due to the inherent difficulty in isolating biochemical quantities of OS-PP-Dol compounds, biosynthetically labeled OS-PP-Dol compounds have served as the donor substrate in most previous enzyme kinetic studies of the OST (*5*, *6*, *12*−*15*).

The OST can utilize dolichol-linked oligosaccharides as donor substrates that range in size between GN_2-PP-Dol and $G_3M_9GN_2$-PP-Dol in vivo and in vitro (*6*, *16*, *17*). However, in vivo utilization of assembly intermediates can be deleterious, as smaller oligosaccharides lack sugar residues that are structurally important for subsequent functions including oligosaccharide-processing reactions in the Golgi complex. The triglucosyl cap on the oligosaccharide is an important determinant during biosynthesis of N-linked glycoproteins (for a review, see ref *18*). Monoglucosylated oligosaccharides on nascent glycoproteins serve as recognition markers for two ER-resident lectin chaperones, calnexin, and calreticulin, which retain nascent glycoproteins in the ER until correctly

† This work was supported by the National Institutes of Health (NIH Grant GM 43768).

* To whom correspondence should be addressed. Phone: (508) 856-5894. Fax: (508) 856-6231. E-mail: Reid.Gilmore@umassmed.edu.

[1] Abbreviations: ALG, asparagine-linked glycosylation; DNJ, 1-deoxynojirimycin-HCl; DTT, dithiothreitol; EDTA, ethylenediaminetetraacetic acid; G3 or $G_3M_9GN_2$-PP-Dol, $Glc_3Man_9GlcNAc_2$-PP-Dol; HPLC, high-pressure liquid chromatography; M9 or M_9GN_2-PP-Dol, $Man_9GlcNAc_2$-PP-Dol; Ni-NTA, nickel nitriloacetic acid; OST, oligosaccharyltransferase, OS-PP-Dol, dolichol-linked oligosaccharide; PAGE in SDS, polyacrylamide gel electrophoresis in sodium dodecyl sulfate; PCR, polymerase chain reaction; PMSF, phenylmethanesulfonyl fluoride; PVDF, polyvinyldifluoride; RER, rough endoplasmic reticulum.

10.1021/bi0111911 CCC: $20.00
Published on Web 09/14/2001

folded as part of a quality control mechanism (for reviews, see refs *19* and *20*). Consequently, the mechanism used by the OST to discriminate between the assembly intermediates and the fully assembled donor substrate has important physiological implications. The solution structure of the triglucosylated high mannose oligosaccharide has revealed that the glucose residues adopt a stable conformation that would be accessible to the OST, processing glucosidases and ER lectins (*21*).

The analysis of yeast *alg* [asparagine-linked glycosylation (*22*)] mutants defective in OS-PP-Dol assembly and the structural characterization of intermediates that accumulate in mammalian cells (*23*, *24*) led to the elucidation of the OS-PP-Dol assembly pathway. OS-PP-Dol assembly is initiated on the cytoplasmic face of the RER by glycosyltransferases that mediate the stepwise transfer of two *N*-acetylglucosamine residues and five mannose residues onto dolichol phosphate (for a review, see ref *25*). OS-PP-Dol assembly is completed within the RER lumen by the glycosyltransferases that add four additional mannose residues and three glucose residues, hence the last seven assembly intermediates (M_5GN_2-PP-Dol to $G_2M_9GN_2$-PP-Dol) reside on the same face of the RER as the catalytic site of the OST. Despite the lumenal location of the OS-PP-Dol assembly intermediates, the fully assembled donor ($G_3M_9GN_2$-PP-Dol) is preferentially utilized by the OST relative to the assembly intermediates (*13*, *26*), consistent with the view that the terminal glucose residue is an important determinant for substrate recognition by the OST (*27*). The mechanism responsible for preferential recognition of the fully assembled donor substrate has been the focus of several studies. Although the relative in vitro transfer rates for $G_3M_9GN_2$-PP-Dol and M_9GN_2-PP-Dol differ by 10−25-fold (*13*, *26*), the K_m values for the two donor substrates were found to be remarkably similar (*13*), suggesting that donor substrate selection cannot be explained by a marked difference in binding affinity. The K_m values for $G_3M_9GN_2$-PP-Dol and GN_2-PP-Dol are also not significantly different (*6*). The observation that the K_m for the peptide substrate is reduced in the presence of $G_3M_9GN_2$-PP-Dol relative to GN_2-PP-Dol (*9*, *15*) has led to the hypothesis that the higher transfer rates for the optimal substrate are explained by a donor substrate-induced conformational change in the peptide binding site (*15*). Given the pronounced difference in the in vitro transfer rates for $G_3M_9GN_2$-PP-Dol relative to M_9GN_2-PP-Dol, one might predict severely reduced in vivo glycosylation by a yeast *alg* mutant (*alg5* or *alg6*) that assembles M_9GN_2-PP-Dol as the largest donor substrate. Instead, the glycoproteins expressed by various *alg* mutants typically show less than a 2-fold reduction in N-linked oligosaccharides per glycoprotein (*25*). Thus, there appears to be a disparity between the relative in vitro transfer rates and the in vivo consequences of a deficiency in $G_3M_9GN_2$-PP-Dol biosynthesis.

Here, we report a detailed steady-state kinetic analysis of the purified yeast OST using the iodinated tripeptide *N*α-Ac-Asn-[^{125}I]Tyr-Thr-NH_2 as the acceptor substrate and highly enriched $G_3M_9GN_2$-PP-Dol and M_9GN_2-PP-Dol as alternative donor substrates. The kinetic experiments revealed substantial deviations from simple Michaelis−Menten enzyme kinetics when OS-PP-Dol was the variable substrate. Possible reasons for the discrepancy between our results and earlier studies reporting that OST activity obeyed Michaelis−Menten kinetics are discussed. Our results disclose unexpected allosteric properties of the enzyme that appear to be of central importance in mediating donor substrate specificity. Kinetic experiments using either oligosaccharide donor as an alternative competitive substrate provide further support for an ordered substrate activation mechanism. This mechanism would explain how the enzyme could select the fully assembled donor substrate from a complex mixture of assembly intermediates, yet transfer nonoptimal donors with relatively high efficiency when $G_3M_9GN_2$-PP-Dol is absent.

MATERIALS AND METHODS

6×His/FLAG-Tagged Ost1p Strains. Standard yeast genetics (*28*) and molecular biology (*29*) techniques were used. A DNA fragment corresponding to the nucleotides 1144−1952 of the *OST1* gene was amplified using *Saccharomyces cerevisiae* genomic DNA as a template. The 5′ PCR primer (CCCAAGCTTGGGAAGATATTCCGAG) contains a *Hin*dIII recognition site. The 3′ PCR primer (TCAGTGATGGTGATGGTGATGACCCTTGTCATCGTCGTCCTTGTAGTCACCACGACCTTCGATGTCTACGTTAGTTACGTTCATGTTC) included sequences encoding a Factor Xa protease cleavage site, and the FLAG and six histidine (6×His) affinity tags. The PCR-product (881 bp) was digested with *Hin*dIII and ligated to the plasmid pRS306OST3-HA3 (*30*) digested with *Hin*dIII and *Msc*I. The final plasmid pRS306ΔOST1-His6 was digested with *Sph*1 and used to transform RGY323 (*MAT*α *ura3−52 leu2-Δ1 lys2−801 ade2−101 trp1-Δ1 his3-Δ200*) (*30*) to obtain the strain designated as RGY350.

Diploid Strain Expressing a 6×His/FLAG-Tagged Stt3p and a HA-Tagged Stt3p. A 5′ PCR primer (CAGAAGCTTTCTTTTACTTCTCTTCGCC) containing a *Hin*dIII recognition site and the sequences corresponding to nucleotides −218 to −193 of the *STT3* gene and a 3′ primer (TCAGTGATGGTGATGGTGATGACCCTTGTCATCGTCGTCCTTGTAGTCACCACGACCTTCGATGTCTACGACTCTCAAGCCTAATTCAGG) were used to obtain a 952 bp PCR product using the plasmid pRS306ΔSTT3-HA3 (*30*) as a template. The 3′ primer encodes a Factor Xa protease cleavage site, the FLAG and 6×His affinity tags, and 21 nucleotides from the *STT3* gene (2352−2372). The PCR product was digested with *Hin*dIII and ligated to *Hin*dIII-*Msc*I-digested pRS306OST3-HA3 to obtain pRS306ΔSTT3-His6. After digestion with *Eco*RI, pRS306ΔSTT3-His6 was used to transform strain RGY326 (*MAT* ***a*** *ura3−52 leu2-Δ1 lys2−801 ade2−101 trp1-Δ1 his3-Δ200*) to uracil prototrophy to obtain RGY360. RGY326 was obtained as one of the wild-type segregants of a diploid strain generated by disruption of the *OST3* gene in YPH274 (*31*).

Two haploid strains, RGY360 and RGY340 (*30*), were subjected to filter mating to obtain a diploid strain designated RGY361 (Mat ***a***/α *ura3−52 leu2-Δ1 lys2−801 ade2−101 trp1-Δ1 his3-Δ200*) which expresses 6×His/FLAG-tagged Stt3p and HA-tagged Stt3p. A mating test was performed to confirm that RGY361 is a diploid.

Digitonin-solubilized extracts of unlabeled RGY360, RGY340, and RGY361 cells were prepared as described (*31*). Nondenaturing immunoprecipitation with anti-FLAG M2

affinity gel (Sigma A1205) and HA.11 affinity matrix (Covance; Richmond, CA) were performed as described except that the immunoprecipitates were not washed with the buffer containing the nonionic detergent Nikkol (*30*).

Purification of the Yeast Oligosaccharyltransferase. Yeast cells expressing 6×His/FLAG-tagged Ost1p were grown at 25 °C in a 3.2 l of YPD media supplemented with adenine (40 μg/mL) until mid log phase (A_{600} of 0.8−1.6). Microsomal membranes were isolated, and then treated with high salt and permeablized with Nikkol as described previously (*32*). The membranes were suspended in 20 mM Tris-Cl (pH 7.4), 1 mM $MgCl_2$, 1 mM $MnCl_2$, 1 mM $CaCl_2$, 75 mM NaCl, 150 mM mannitol, 1 mM phenylmethylsulfonyl fluoride (PMSF) and a protease inhibitor mixture (as defined in ref *32*) to give a concentration of ~4 equiv/μL (for the definition of equiv, see ref *32*). DNase I (Boehringer Mannheim, no. 104132) was added to give a final concentration of 0.2 mg/mL and the membranes were incubated for 45 min at room temperature (*34*). Thereafter, all the procedures were performed at 4 °C. After adjusting the suspended membranes to 1.5% digitonin (Calbiochem, no. 3004) and 0.5 M NaCl, the extract was incubated for 30 min by end-over-end rotation. After an insoluble residue was separated by centrifugation for 30 min at 184000*g* in a Ti50.2 rotor, glycoproteins in the digitonin extract (~0.3 equiv/μL) was batch-absorbed to dimethylpimelimidate cross-linked ConA-Sepharose CL-4B as described (*32*). Glycoproteins were eluted as described (*32*), except that the elution buffer lacked $MnCl_2$. The eluate (~76 mL) from the ConA-Sepharose was diluted to 100 mL to give a final concentration of 20 mM Tris-Cl (pH 8), 0.5 M NaCl, 15 mM imidazole, 10 mM $MgCl_2$, 0.15% digitonin, 34 μM egg phosphatidylcholine, and 0.1 mM PMSF. The eluate was then incubated for about 16 h with 6.5 mL of nickel nitriloacetic acid (Ni-NTA) agarose (Qiagen) resin equilibrated with Ni-NTA buffer [20 mM Tris-Cl (pH 8), 10 mM $MgCl_2$, 0.15% digitonin, 34 μM egg phosphatidylcholine, 0.5 M NaCl, and 5 mM imidazole]. The Ni-NTA agarose was poured into a 1.5-cm-diameter column, washed with Ni-NTA buffer, and the bound proteins were eluted with 20 mM Tris-Cl (pH 8), 1 mM $MgCl_2$, 1 mM $MnCl_2$, 0.125% digitonin, 34 μM egg phosphatidylcholine, 0.3 M NaCl and 350 mM imidazole. The second and third 6.5 mL fractions were pooled as they contained >90% of the hexahistidine-tagged Ost1p as determined by protein immunoblotting (see below). Pooled fractions were subjected to diafiltration using a BioMax 10K centrifugal filter (Millipore) as described by the manufacturer to exchange the protein into 20 mM Tris-Cl (pH 7.4), 1 mM $MgCl_2$, 1 mM $MnCl_2$, 0.125% digitonin, 34 μM egg phosphatidylcholine, 50 mM NaCl.

Protein Immunoblots. Purified OST was resolved by SDS−PAGE and stained with Coomassie Blue or was transferred to PVDF membranes. The membranes were probed with antibodies to Ost1p, Ost2p, Ost6p, Wbp1p, Swp1p, the FLAG epitope (Eastman Kodak), and the 6×His epitope (Qiagen) as described (*35*). Horseradish peroxidase-conjugated secondary antibodies were visualized using enhanced chemiluminescence (ECL Western blotting detection kit, Amersham Corp.).

Oligosaccharyltransferase Assays and HPLC Analysis of Glycopeptides. Oligosaccharyltransferase assays using the purified yeast OST were performed essentially as described previously (*33*) except that the assays were incubated for 30 min at 25 °C, unless otherwise stated. When noted, the assays were supplemented with a glucosidase inhibitor [1.3 mM 1-deoxynojirimycin-HCl (DNJ, Calbiochem)] and/or a mannosidase inhibitor [1.3 mM 1-deoxymannojirimycin-HCl (DMJ, Calbiochem)]. The OST assays were terminated by the addition of ice-cold Stop Mix 1 (106 μL of 9% Nikkol and 10 mM EDTA) followed by ice-cold Stop Mix 2 (1 mL of 50 mM Tris-Cl, pH 6.7, 1 M NaCl, 1 mM $MnCl_2$, 3 mM $MgCl_2$, 1 mM $CaCl_2$, and 0.3% Nikkol). Glycopeptide products were isolated and either quantified directly by gamma counting, or eluted and resolved according to oligosaccharide size using a Varian/Rainin aminopropyl silica HPLC column (*33*). Assays of OST activity in intact canine microsomes were conducted using a 1 mL assay volume that contained ~800 μg of canine rough microsomes, 5 μM Nα-Ac-Asn-[^{125}I]Tyr-Thr-NH_2, 20 mM Tris-Cl, pH 7.4, 135 mM NaCl, 1 mM $MnCl_2$, 3 mM $MgCl_2$, 1 mM DTT, 1× protease inhibitor cocktail and 1.35 mM DNJ. To examine the initial rates of glycopeptide formation at 25 °C, the microsomes (100 μL) and the remaining components (900 μL) were preincubated at 25 °C in separate tubes for 5 min before mixing at 0 time. Aliquots (50 or 100 μL) of the assay were removed at frequent time intervals, and the OST assays were terminated as described above.

Isolation of Dolichol-Oligosaccharides. $G_3M_9GN_2$-PP-Dol was isolated from porcine pancreas by sequential extraction with organic solvents and further purified by preparative aminopropyl silica HPLC as described (*33*). To obtain M_9GN_2-PP-Dol, rough microsomal membranes from canine pancreas (*36*) or porcine pancreas were incubated at 37 °C for 2 or 1 h, respectively, to allow deglucosylation of $Glc_3Man_9GlcNAc_2$-PP-Dol by endogenous glucosidases. The M_9GN_2-PP-Dol was extracted from the membranes and subsequently purified by preparative aminopropyl silica HPLC (*33*).

The concentration and composition of the dolichol oligosaccharide preparations were determined using the OST endpoint assay (*33*). The results of the OST endpoint assay were confirmed by a monosaccharide analysis performed by the Complex Carbohydrate Research Center at the University of Georgia using Dionex high pH-anion exchange chromatography (*33*).

Analysis of Kinetic Data. Steady-state velocity equations for OST-catalyzed tripeptide glycosylation using single dolichol oligosaccharides (Figure 5) or dolichol oligosaccharide mixtures (Figures 6 and 7) were obtained by making the rapid-equilibrium assumption (*37*). The kinetic parameters for the tripeptide acceptor were determined by a nonlinear least-squares fit of the kinetic data to the Michaelis−Menten equation using Kaleidagraph 3.5 (Synergy Software). The kinetic parameters for the dolichol-oligosaccharide donor were determined by a nonlinear least-squares fit of the kinetic data to eq 1 for a substrate-activated bireactant system (ref *37*, and see Figure 5), using Kaleidagraph 3.5 software. The term K_s is the intrinsic dissociation constant for OS-PP-Dol binding to an activator site. The terms [E_t], [S], and [P] are the concentrations of enzyme, OS-PP-Dol and acceptor tripeptide respectively while V_s is k_{cat}. The term α is an interaction factor that describes how binding of OS-PP-Dol to the activator site influences the dissociation constant for OS-PP-Dol binding to the catalytic

site. K_p is the intrinsic dissociation constant for binding of the acceptor tripeptide to the catalytic site. The K_p values derived from kinetic experiments where the tripeptide was the variable substrate were used to reduce the number of variable during curve fitting of the dolichol oligosaccharide kinetic data.

$$v = \frac{\left(\frac{[E_t]V_S[P][S]^2}{\alpha K_S{}^2 K_p}\right)}{1 + \frac{[S]}{K_S} + \frac{[S]^2}{\alpha K_S{}^2} + \frac{[S]^2[P]}{\alpha K_S{}^2 K_p} + \frac{[S][P]}{K_S K_p}} \quad (1)$$

The kinetic parameters for dolichol oligosaccharide competition experiments were calculated by a nonlinear least-squares fit of the kinetic data to steady-state rate equations for the formation of $G_3M_9GN_2$-NYT (v_{G3}) and M_9GN_2-NYT (v_{M9}) (eqs 2 and 3; see Figure 6). The terms $[G_3]$ and $[M_9]$ are the concentrations of $G_3M_9GN_2$-PP-Dol and M_9GN_2-PP-Dol, respectively. The terms K_{pG3} and K_{pM9} are the dissociation constants for the tripeptide acceptor when the activator site is occupied by $G_3M_9GN_2$-PP-Dol or M_9GN_2-PP-Dol, respectively. V_{GG}, V_{GM}, V_{MG}, and V_{MM} are k_{cat} terms that specify which donor substrate is bound to the catalytic (first subscript) and activator sites (second subscript). The terms α, β, γ, and δ are homotropic (α and δ) and heterotropic (β and γ) interaction factors that describe how binding of OS-PP-Dol to the activator site influences the dissociation constant for OS-PP-Dol binding to the catalytic site. Interaction factors are defined in the text. D1 and D2 in eqs 2 and 3 are defined in eqs 4 and 5.

$$v_{G3} = \frac{\left(\frac{[E_t]V_{GG}[G_3]^2[P]}{\alpha K_{G3}{}^2 K_{pG3}} + \frac{[E_t]V_{GM}[G_3][M_9][P]}{\beta K_{G3} K_{M9} K_{pM9}}\right)}{(1 + D_1 + D_2)} \quad (2)$$

$$v_{M9} = \frac{\left(\frac{[E_t]V_{MM}[M_9]^2[P]}{\delta K_{M9}{}^2 K_{pM9}} + \frac{[E_t]V_{MG}[G_3][M_9][P]}{\gamma K_{M9} K_{G3} K_{pG3}}\right)}{(1 + D_1 + D_2)} \quad (3)$$

$$D_1 = \left(\frac{[G_3]}{K_{G3}}\right)\left(1 + \frac{[G_3]}{\alpha K_{G3}} + \frac{[G_3][P]}{\alpha K_{G3} K_{pG3}} + \frac{[M_9]}{\gamma K_{M9}} + \frac{[P]}{K_p G_3} + \frac{[M_9][P]}{\gamma K_{M9} K_{pG3}}\right) \quad (4)$$

$$D_2 = \left(\frac{[M_9]}{K_{M9}}\right)\left(1 + \frac{[M_9]}{\delta K_{M9}} + \frac{[M_9][P]}{\delta K_{M9} K_{pM9}} + \frac{[G_3]}{\beta K_{G3}} + \frac{[P]}{K_{pM9}} + \frac{[G_3][P]}{\beta K_{G3} K_{pM9}}\right) \quad (5)$$

Due to the large number of variables, the rate equations for $G_3M_9GN_2$-NYT and M_9GN_2-NYT formation in the competition experiments do not yield unique solutions unless one substitutes several variables (V_{GG}, V_{MM}, K_{pG3}, K_{PM9}, α, δ, K_{M9}, and K_{G3}) with the values derived from kinetic experiments in which a single OS-PP-Dol compound was the variable substrate. To further reduce the number of variables, we made the simplifying assumption that the k_{cat} was determined by the OS-PP-Dol molecule bound to the catalytic site (e.g., $V_{GG} = V_{GM}$ and $V_{MM} = V_{MG}$). The quality of curve fits for both products was evaluated by the calculation of residuals (not shown).

The OST kinetics data was also fit to eq 6 for a bireactant system with a random order of binding. The variables are as defined above for eq 1 except that K_s is the Michaelis constant for the OS-PP-Dol donor, while an interaction factor (a) defines the allosteric interactions between the donor and acceptor substrates.

$$v = \frac{\left(\frac{[E_t]V[S][P]}{aK_S K_p}\right)}{1 + \frac{[P]}{K_p} + \frac{[S]}{K_S} + \frac{[S][P]}{aK_S K_p}} \quad (6)$$

The kinetic data obtained in the OS-PP-Dol competition experiments were analyzed using eqs 7 and 8, where K_{G3}, V_G, and K_{M9} and V_M are Michaelis constants and V_{max} values for $G_3M_9GN_2$-PP-Dol and M_9GN_2-PP-Dol as the respective donor oligosaccharides. The ratio of the interaction factors (a and b) specify the effect of OS-PP-Dol donor structure on the peptide binding affinity (K_p).

$$v_{G3} = \frac{\left(\frac{[E_t]V_G[G_3][P]}{aK_{G3}K_p}\right)}{1 + \frac{[P]}{K_p} + \frac{[G_3]}{K_{G3}} + \frac{[M_9]}{K_{M9}} + \frac{[G_3][P]}{aK_{G3}K_p} + \frac{[M_9][P]}{bK_{M9}K_p}} \quad (7)$$

$$v_{M9} = \frac{\left(\frac{[E_t]V_M[M_9][P]}{bK_{M9}K_p}\right)}{1 + \frac{[P]}{K_p} + \frac{[G_3]}{K_{G3}} + \frac{[M_9]}{K_{M9}} + \frac{[G_3][P]}{aK_{G3}K_p} + \frac{[M_9][P]}{bK_{M9}K_p}} \quad (8)$$

RESULTS

Oligosaccharide Donor Preference in Intact Microsomes. It is well accepted that the triglucosylated dolichol-linked oligosaccharide $G_3M_9GN_2$-PP-Dol is the optimal donor substrate when the OST is assayed in detergent solution. Before embarking upon a kinetic analysis of the purified yeast oligosaccharyltransferase, we first asked whether the OST in an intact membrane transfers $G_3M_9GN_2$-PP-Dol more rapidly than OS-PP-Dol compounds that lack the terminal glucose and mannose residues. To address this question, we first determined the oligosaccharide composition of OS-PP-Dol samples isolated from several different preparations of canine rough microsomes using the OST endpoint assay (*33*). A microsome preparation that had the following endogenous OS-PP-Dol composition was selected to measure donor substrate preference in the intact membrane: $M_{3-7}GN_2$-PP-Dol, 4.7%; M_8GN_2-PP-Dol, 3.3%; M_9GN_2-PP-Dol, 27.9%; $G_1M_9GN_2$-PP-Dol, 18.7%, $G_2M_9GN_2$-PP-Dol, 18.2%, $G_3M_9GN_2$-PP-Dol, 27.2%. In the initial experiment, the membrane permeable acceptor tripeptide Nα-Ac-Asn-[^{125}I]Tyr-Thr-NH_2 was added to an OST assay that contained the intact microsomes, lacked detergent, and was supplemented with the glucosidase inhibitor deoxynojirimycin (Figure 1A). Aliquots of the assay were quenched at frequent intervals

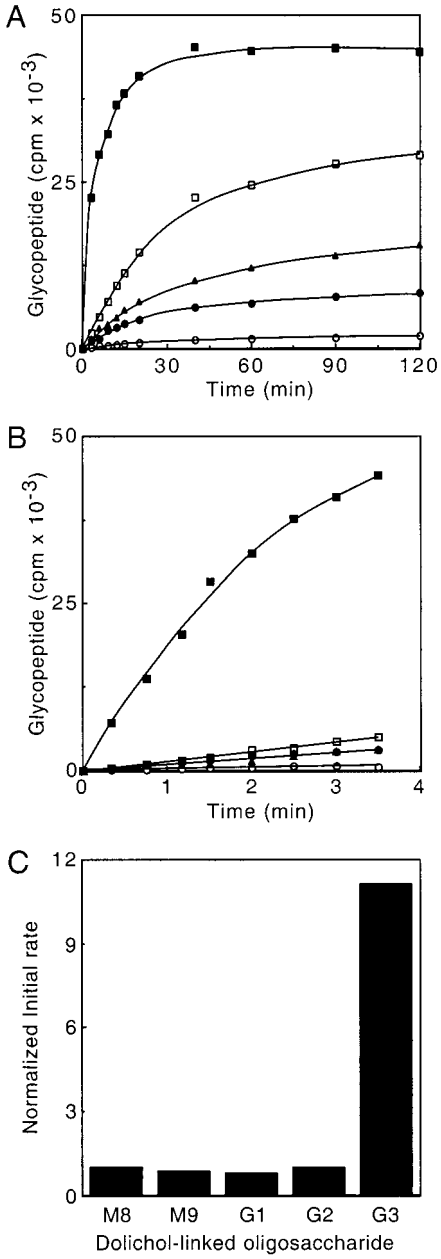

FIGURE 1: Initial rates of glycopeptide formation by the OST in intact canine microsomes. (A and B) A 1 mL oligosaccharyltransferase assay (see Materials and Methods) contained 100 equiv of canine microsomes (~800 μg of protein), 5 μM Nα-Ac-Asn-[^{125}I]-Tyr-Thr-NH_2 and 1.35 mM DNJ. Aliquots (50 μL in panel A, 100 μL in panel B) were removed at frequent time intervals and assays were terminated with an ice-cold detergent-EDTA solution. Radiolabeled glycopeptide products were isolated, and resolved by HPLC to quantify $G_3M_9GN_2$-NYT [G3 (■)], $G_2M_9GN_2$-NYT [G2 (●)], $G_1M_9GN_2$-NYT [G1 (▲)], M_9GN_2-NYT [M9 (□)], and M_8GN_2-NYT [M8 (○)]. (C) The initial rates of glycopeptide formation, as determined from the data in panel B, were divided by the OS-PP-Dol composition of the membranes, as determined by a composition analysis of isolated OS-PP-Dol. The bar graph shows the normalized initial transfer rate for the five most abundant OS-PP-Dol compounds in the membrane preparation.

during a 2 h incubation. The glycopeptide products that were collected by binding to ConA-Sepharose were eluted and resolved according to oligosaccharide size by HPLC using an aminopropyl silica column (*33*). Examination of the time course data revealed that $G_3M_9GN_2$-NYT reached a plateau value more rapidly than any other product, accounting for greater than 50% of the total product present at the earliest time point. A second abbreviated 3 min time-course experiment was conducted using a 2-fold greater quantity of microsomes (Figure 1B) to determine initial transfer rates for the five largest OS-PP-Dol compounds present in the microsomes. As anticipated, the transfer rate for $G_3M_9GN_2$-PP-Dol was more rapid than the other OS-PP-Dol compounds. The initial transfer rates derived from Figure 1B were normalized by dividing the rates by the percentage of each OS-PP-Dol compound in the donor pool. The normalized transfer rates (Figure 1C) reveal that within the intact membrane the transfer rate for $G_3M_9GN_2$-PP-Dol is roughly 11-fold faster than for donor oligosaccharides that lack the three glucose residues. The normalized transfer rate for these other compounds (M_8GN_2-PP-Dol to $G_2M_9GN_2$-PP-Dol) is essentially identical, suggesting that the OST does not discriminate between different compounds that lack the terminal glucose residue.

Purification of the 6×His-Tagged Yeast OST Complex. The yeast OST is an oligomer composed of eight nonidentical subunits (Stt3p, Ost1p, Wbp1p, Swp1p, Ost3p/Ost6p, Ost2p, Ost5p, Ost4p) ranging in molecular weight from 78K to 3.6K (*30*, *38*, *39*). The OST has been purified from several vertebrate sources including canine pancreas (*40*), hen oviduct (*41*), human liver (*42*), and porcine liver (*15*). Although the purified vertebrate OST complexes appear to have fewer total subunits (ribophorin I, ribophorin II, OST48, and DAD I), protein sequence databases contain entries with significant homology to all of the yeast OST subunits with the exception of Ost5p. The apparent differences in subunit composition between the fungal and vertebrate enzymes may be due to subunit dissociation during purification or differences in polypeptide detection methods. We chose the yeast enzyme for kinetic analysis due to the greater certainty that all relevant subunits are present in the purified enzyme preparation.

Two affinity tags, an eight-residue FLAG epitope and a 6×His motif, were appended to the C-terminus of Ost1p to allow purification of the yeast OST by Ni-NTA affinity chromatography. A one-step allele replacement technique was used to substitute the epitope-tagged *OST1* gene for its chromosomal copy in a haploid wild-type yeast strain. Replacement of the wild-type Ost1 protein with the epitope-tagged Ost1 protein had no detectable effect on cell growth or on in vivo OST activity indicating that the epitope-tagged protein is fully functional (not shown). Purification of the yeast OST complex containing the identical dual affinity tag on Ost1p, expressed under the control of *CUP1* promoter, has been reported previously (*43*). Here, the epitope-tagged Ost1p was expressed from its own promoter to minimize the presence of unassembled Ost1p in the preparation.

Protein immunoblots using antibodies specific for the two affinity tags (anti-6×His or anti-FLAG) revealed a glycoform doublet of approximately 64K (*32*) in cell extracts prepared from the epitope-tagged strain (not shown). Coomassie Blue staining of the OST complex purified from the strain expressing epitope-tagged Ost1p revealed the presence of nine polypeptides with apparent molecular weights corresponding to the previously characterized subunits of the yeast OST (*30*, *38*). Protein immunoblots of the purified OST were probed with antibodies to Ost1p, Wbp1p, Swp1p, Ost2p, and Ost6p to confirm that the affinity-tag purified complex had

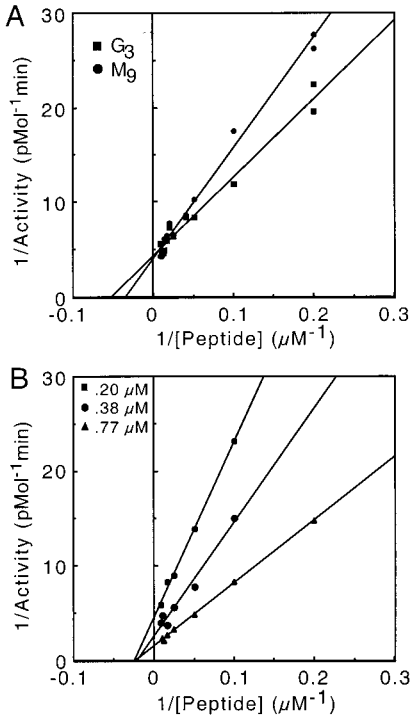

FIGURE 2: Effect of donor substrate structure and concentration on the kinetic parameters for the tripeptide acceptor. (A) OST activity was assayed using a constant saturating concentration of $G_3M_9GN_2$-PP-Dol (510 nM) or M_9GN_2-PP-Dol (940 nM). Lineweaver−Burk plots of 1/activity versus 1/[tripeptide]. Data from two separate experiments are combined. (B) OST activity was assayed using either a nonsaturating (0.2 and 0.38 μM) or a saturating (0.77 μM) concentration of $G_3M_9GN_2$-PP-Dol. Lineweaver−Burk plots of 1/activity versus 1/[tripeptide].

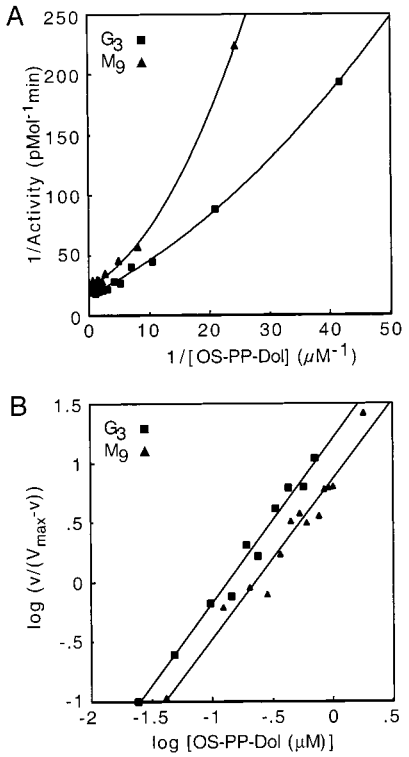

FIGURE 3: Kinetic parameters for the oligosaccharide donor substrate. OST activity was assayed using 5 μM Nα-Ac-Asn-[^{125}I]-Tyr-Thr-NH_2 and variable concentrations of $G_3M_9GN_2$-PP-Dol (■) or M_9GN_2-PP-Dol (▲). (A) Lineweaver−Burk plots of 1/activity versus 1/(OS-PP-Dol) were nonlinear for $G_3M_9GN_2$-PP-Dol (■) and M_9GN_2-PP-Dol (▲). The data shown was typical of five separate experiments for each donor substrate. (B) The intercepts of the curved plots at the $1/v$-axis were used to calculate $1/V_{max}$. Hill plots for the data points ranging between 0.1 and 0.9 V_{max} were constructed to calculate the Hill coefficients for the enzyme when $G_3M_9GN_2$-PP-Dol (■) or M_9GN_2-PP-Dol (▲) was the donor substrate.

the normal subunit composition (not shown). The concentration of the purified OST was estimated by the Coomassie blue staining intensity of the individual subunits relative to protein molecular weight markers of known concentration (not shown).

OST Assays Using Purified Yeast OST and Purified OS-PP-Dol. To investigate the steady-state kinetics of the oligosaccharyltransferase, OST assays were performed using known quantities of purified OS-PP-Dol (Figure 3B in ref *33*) as the donor substrate and a synthetic tripeptide (N^{α}-Ac-Asn-[^{125}I]Tyr-Thr-NH_2) with a high specific activity (15000−25000 cpm/pmol) as the acceptor substrate. The enzyme concentration (0.29 nM) and the length of the incubation (30 min) were adjusted to ensure that the quantity of glycopeptide product did not exceed 10% of the initial donor substrate. The oligosaccharide $G_3M_9GN_2$-PP-Dol accounts for ∼95% of the donor substrate in the $G_3M_9GN_2$-PP-Dol preparation; traces of $G_2M_9GN_2$-PP-Dol and $G_1M_9GN_2$-PP-Dol are the primary contaminants (*33*). The oligosaccharide M_9GN_2-PP-Dol accounts for 85−90% of the donor substrate in the M_9GN_2-PP-Dol preparation; $G_1M_9GN_2$-PP-Dol and M_8GN_2-PP-Dol are the contaminants, while $G_3M_9GN_2$-PP-Dol is undetectable (*33*). Product formation was linear with time for at least an hour (not shown). We have shown that the yeast OST remains active during a 48 h OST endpoint assay and that the OS-PP-Dol substrate is stable in our assay buffer (*33*). Therefore, under our assay conditions, substrate depletion or substrate and product degradation are unlikely. The linear time course of glycopeptide formation suggests that the assay products (glycopeptide and the dolichol pyrophosphate) are not inhibitors. Experimental evidence that glycopeptides are not inhibitors has been presented by other investigators (*9*). The detergent digitonin is present in our assay at a concentration (50 μM) that is below the critical micelle concentration (∼75 μM), and our assay contains 1.35 mM egg yolk phosphatidylcholine. Consequently, the OST and the dolichol oligosaccharide are incorporated into liposomes that elute in the void volume of a Sepharose CL-2B gel filtration column consistent with the presence of large proteoliposomes (not shown).

Kinetic Parameters for the Tripeptide Acceptor Substrate. It has been demonstrated that OST catalyzes a bisubstrate reaction (*44*, *45*) that requires the simultaneous presence of both the donor and the acceptor substrates to give the glycopeptide product. Saturation curves for the $G_3M_9GN_2$-PP-Dol and M_9GN_2-PP-Dol donor substrates obtained using 5 μM tripeptide (N^{α}-Ac-Asn-[^{125}I]Tyr-Thr-NH_2) as the constant substrate yielded preliminary estimates for the K_m value for the donor substrates of approximately 150 nM. Accordingly, to determine the kinetic parameters for the tripeptide acceptor, the OST assays contained a saturating concentration of $G_3M_9GN_2$-PP-Dol (510 nM) or M_9GN_2-PP-Dol (940 nM) and the tripeptide substrate concentration was varied between 5 and 50 μM. Since the maximum concentration of I^{125}-labeled tripeptide in the assay was 10 μM, appropriate amounts of unlabeled tripeptide were added to

each assay to obtain total tripeptide concentrations up to 50 μM. The final specific radioactivity for the I^{125}-labeled glycopeptide products was corrected accordingly. Linear Lineweaver−Burk plots (Figure 2A) and hyperbolic Michaelis−Menten curves (not shown) were obtained and apparent K_m and V_{max} values were calculated. A slightly higher affinity for the tripeptide substrate was observed when $G_3M_9GN_2$-PP-Dol ($K_m = 21.3$ μM) was the donor substrate compared to when M_9GN_2-PP-Dol ($K_m = 31.5$ μM) was the substrate. This 1.5-fold difference in apparent K_m was small, yet reproducible, and was derived from experiments where both donor substrates were tested in a single experiment. As expected from Figure 2A, Hill plots of the experimental data yielded Hill coefficients ranging between 0.95 and 1.05 (not shown), indicating the presence of a single acceptor tripeptide binding site. Our results confirmed earlier kinetic studies of the OST (*5*, *9*, *14*) showing that the enzyme has a single tripeptide binding site with a K_m of roughly 20 μM.

Double reciprocal plots, which were obtained for the tripeptide substrate at three different fixed concentrations of $G_3M_9GN_2$-PP-Dol (0.20, 0.38, and 0.77 μM), yielded lines that intersected to the left of the 1/activity-axis and on the 1/*S*-axis (Figure 2B), hence the apparent K_m value for the tripeptide is not influenced by the concentration of the donor substrate. Similar results were obtained when M_9GN_2-PP-Dol was the donor substrate.

Cooperative Binding of Dolichol Oligosaccharides to the OST. The titration curves for OS-PP-Dol donor substrates were obtained using a fixed concentration of 5 μM I^{125}-labeled tripeptide as the acceptor substrate, while varying the donor substrate concentration between 25 nM and 2 μM. The two oligosaccharide donors ($G_3M_9GN_2$-PP-Dol and M_9GN_2-PP-Dol) were tested five times each using the OST assay conditions described above. The results of a typical experiment, in which 10 different concentrations of donor substrate were tested, are shown in Figure 3A. In contrast to the results we obtained when the tripeptide acceptor was the variable substrate (Figure 2A), the Lineweaver−Burk plots obtained for $G_3M_9GN_2$-PP-Dol and M_9GN_2-PP-Dol were nonlinear (Figure 3A). As expected from the data presented in Figure 3A, plots of OST activity versus OS-PP-Dol concentration are sigmoidal rather than hyperbolic. Although the upward curvature of the double reciprocal plots was apparent at both low and high substrate concentrations, the deviation from linearity would be far less obvious if a narrow concentration range of OS-PP-Dol had been tested (e.g., 0.1−1.5 μM). Apparent V_{max} values were determined from the 1/*V* intersect of the nonlinear Lineweaver−Burk plots (Figure 3A). The kinetic data for the donor substrates was then analyzed using the Hill equation, and the data from typical experiments is presented graphically in Figure 3B. The slopes of the Hill plots between the points corresponding to $0.1V_{max}$ and $0.9V_{max}$ were 1.38 and 1.33, respectively for $G_3M_9GN_2$-PP-Dol and M_9GN_2-PP-Dol (Figure 3B), suggesting cooperative binding of the donor oligosaccharide to the enzyme.

OST Complex Does Not Form Stable Higher-Order Oligomers in Detergent Solution. Sigmoidal binding kinetics for the donor oligosaccharide could be explained by the presence of two identical or structurally related subunits in the yeast OST complex. However, the yeast OST is an oligomer composed of eight nonidentical subunits (Ost1p, Ost2p, Ost3p, Ost4p, Ost5p, Wbp1p, Swp1p, and Stt3p) that are present in an equimolar ratio (*30*). With the exception of Ost6p (*39*), an Ost3p homologue, that replaces Ost3p in a second less abundant form of the enzyme, there is no obvious primary sequence homology or predicted secondary structural homology between any of the eight subunits. The presence of more than one OS-PP-Dol binding site, as suggested by kinetic experiments described here, could also arise if the OST octamer forms higher-order oligomers. To address this possibility, we constructed a diploid yeast strain that expresses two different epitope-tagged forms of the Stt3p subunit. The expression of the 6×His/FLAG-tagged Stt3p and HA-tagged Stt3p in the two haploid parents was confirmed by probing protein immunoblots of cell extracts with anti-His (Figure 4A, lanes a and b) or anti-HA antibodies (Figure 4B, lanes a and b). As expected, the diploid strain expressed both tagged forms of Stt3p (Figure 4, panels A and B, lane c). Digitonin extracts that were prepared from the two parental strains and the diploid strain were subjected to sequential nondenaturing immunoprecipitation using the anti-FLAG antibody followed by immunoprecipitation of the initial anti-FLAG supernatant with the anti-HA antibody. It has been previously shown that the OST complex is stable under the conditions used for nondenaturing immunoprecipitation (*30*). The immunoprecipitated proteins were resolved by PAGE in SDS and subjected to protein immunoblot analysis using antibodies specific for the HA or His affinity tags (Figure 4, panels A and B, lanes d−j). If the OST complex forms higher order oligomers in detergent solution, a significant proportion of the HA-tagged Stt3p should be recovered in the anti-FLAG immunoprecipitate when extracts from the diploid (Figure 4B, lane f) but not the haploid strains (Figure 4B, lanes d and e) are tested. Instead, only nonspecific background bands were detected in the anti-HA protein immunoblot (Figure 4B, lanes d−f). OST complexes containing the HA-tagged Stt3 sub-

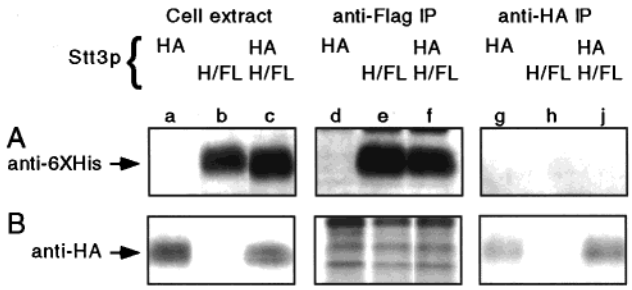

FIGURE 4: Immunoprecipitation of OST complexes using epitope-tagged Stt3p subunits. Digitonin solubilized total cell extracts from haploid cells that express either HA-tagged (HA) (a, d, and g) or 6×His/FLAG-tagged (H/FL) Stt3p (b, e, and h) or from diploid cells that express both (c, f, and j) were either resolved directly by 12% PAGE in SDS (a, b, and c) or were subjected to nondenaturing immunoprecipitation using an anti-FLAG antibody before electrophoresis (d, e, and f). The supernatants from the initial immunoprecipitation with anti-FLAG antibodies were precipitated using anti-HA antibody before electrophoresis (g, h, and j). All the samples (a−j) were divided into two aliquots and the proteins were resolved on duplicate 12% SDS−polyacrylamide gels. After transfer of the proteins to PVDF membranes, the blots were probed either with an anti-6×His antibody (panel A) or an anti-HA antibody (panel B). The migration position for the epitope-tagged Stt3 protein is shown with arrows. The several bands in lanes d−f in panel B are all nonspecific reaction products as they were present in samples prepared from the haploid strain that does not express the HA-tagged Stt3p subunit (lane e).

units were recovered in the second immunoprecipitate (Figure 4B, lanes g and j), and these complexes lacked 6×His/FLAG-tagged Stt3p subunits (Figure 4A, lane j). Thus, we were not able to obtain evidence that there are higher-order forms of the OST complex that contain more than one Stt3p subunit. These results are consistent with previous estimates of the native molecular weight of the OST complex obtained by hydrodynamic methods (*32*) and suggest that cooperative binding of OS-PP-Dol to the OST may involve nonequivalent binding sites within the octamer.

Dolichol-Oligosaccharide Activation of the OST. The contrast between hyperbolic and sigmoidal enzyme velocity plots for the acceptor tripeptide and the oligosaccharide donor led us to consider a substrate activation model as the kinetic mechanism of the enzyme (Figure 5A). A substrate-activated enzyme would have at least two nonequivalent substrate binding sites: a catalytic (C) site and one or more activator or regulatory (R) site(s) (*37*). Binding of the donor substrate to the catalytic and regulatory sites could occur by an ordered or random mechanism. In a strictly ordered mechanism, binding of the substrate to the regulatory site renders the catalytic site accessible by inducing a conformational change (*37*). If binding is random, the donor substrate could bind to the catalytic or regulatory sites randomly and independently (*37*). Steady-state rate equations derived using the ordered reaction mechanism predict sigmoidal enzyme kinetics with a Hill coefficient of ~1.36 (between 0.1 and 0.9 V_{max}) regardless of the value of α (*37*). Random, independent binding of a substrate to the activator and catalytic sites also yields sigmoidal enzyme kinetics, but the Hill coefficient is closer to 1.15. The ordered mechanism depicted in Figure 5A would be consistent with the observation that the structure ($G_3M_9GN_2$-PP-Dol vs M_9GN_2-PP-Dol), but not the concentration, of the oligosaccharide donor effects the apparent K_m for the tripeptide acceptor. Once OS-PP-Dol binds to the activator site, the model in Figure 5A specifies a random order of substrate binding to the catalytic site. Consequently, the apparent K_m for the tripeptide acceptor would be relatively insensitive to changes in the concentration of the dolichol oligosaccharide donor.

Upon the basis of the preceding arguments, the reaction equilibria (Figure 5A) were written assuming an ordered mechanism, in which the OS-PP-Dol substrate binds to the regulatory site first with an affinity K_s. Binding of a second donor substrate to the catalytic site of the enzyme−activator complex is cooperative with a binding affinity of αK_s, where α can be less, equal to, or greater than 1. The K_p values used for curve fitting were as determined in Figure 2A. Each of five kinetic experiments using $G_3M_9GN_2$-PP-Dol as the variable substrate were initially analyzed separately to obtain values for V_s, K_s, and α. The V_s values obtained for the individual experiments were used to scale the five data sets so they could be combined as shown in Figure 5B. The five experiments using M_9GN_2-PP-Dol as the variable substrate were analyzed using the same procedure, and the combined kinetics data is presented in Figure 5C. The steady-state rate eq 1 for the ordered, substrate-activated bireactant system provides a good fit for the experimental data for both dolichol-oligosaccharide donors.

A comparison of the parameters (V_s, K_s, K_p and α) used to fit the experimental data suggests that the greater transfer

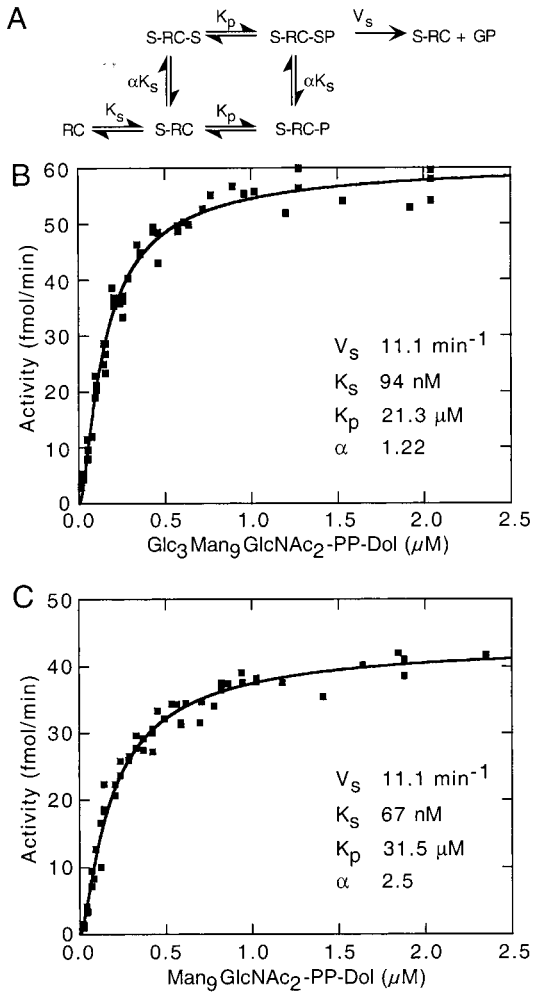

FIGURE 5: Cooperative binding of donor substrates to the OST. (A) A model for a substrate activation mechanism wherein binding of OS-PP-Dol to the regulatory site (R) is a prerequisite for binding of OS-PP-Dol to the catalytic site (C). K_s and αK_s are the affinity constants for binding of the donor substrate (S) to the regulatory and the catalytic sites, respectively. The donor substrate can be either $G_3M_9GN_2$-PP-Dol or M_9GN_2-PP-Dol. Binding of a second donor substrate is defined by an interaction factor α (α > 0). K_p is the affinity constant of the acceptor substrate peptide (P). A random order of binding of the donor (S) and acceptor (P) substrates to the catalytic site is depicted. (B and C) Saturation curves for $G_3M_9GN_2$-PP-Dol (B) and M_9GN_2-PP-Dol (C) were obtained at 5 μM Nα-Ac-Asn-[^{125}I]Tyr-Thr-NH_2. Data points from five different experiments were combined after scaling to correct for experimental variations in apparent V_{max}. The curves were obtained by fitting the data to eq 1 (see Materials and Methods) which was derived according to the equilibria in panel A.

rates for $G_3M_9GN_2$-PP-Dol relative to M_9GN_2-PP-Dol are primarily caused by the difference in K_p, not a difference in k_{cat} (V_s). The apparent K_s values (Figure 5, panels B and C) for $G_3M_9GN_2$-PP-Dol and M_9GN_2-PP-Dol (94 and 67 nM, respectively) were remarkably similar given the anticipated preference for the $G_3M_9GN_2$-PP-Dol donor substrate. A 1.5-fold preference for the $G_3M_9GN_2$-PP-Dol donor substrate was revealed by a comparison of the binding affinities to the catalytic site; the apparent K_m (e.g., αK_s) for $G_3M_9GN_2$-PP-Dol is 115 nM, while the apparent K_m for M_9GN_2-PP-Dol is 168 nM. Although less satisfactory, the experimental data could also be fit using equations derived for a random order of OS-PP-Dol binding to the activator and catalytic sites, thus we could not readily discriminate between these two

models based upon experiments using a single dolichol oligosaccharide donor.

One prediction of the model in Figure 5A is that the kinetic parameters for the dolichol oligosaccharide donor (α and K_s) should not be influenced by the concentration of the tripeptide substrate. In an experiment using several fixed concentrations of the acceptor tripeptide (5, 10, 30, and 50 μM), we observed that the binding affinity for the $G_3M_9GN_2$-PP-Dol was not significantly altered by the tripeptide concentration (not shown). Since the apparent binding affinity for both the donor and acceptor substrates was not effected by changing the concentration of the other substrate, this suggests a random order of binding of the acceptor and donor substrates to the catalytic site.

Competition between $G_3M_9N_2$-PP-Dol and M_9GN_2-PP-Dol as alternative Substrates. It is well documented that the yeast OST transfers the glucosylated donor substrate 5−20-fold more rapidly than nonglucosylated substrates in vitro (*6*, *13*). Although in vivo transfer rates are difficult to estimate, *alg* mutants that assemble OS-PP-Dol donors lacking the terminal glucose residue synthesize glycoproteins that carry fewer N-linked oligosaccharides (*22*, *46*). The rather modest difference (~1.5-fold) in substrate binding affinity that we observe here for the two donor substrates cannot readily explain the preferential utilization of $G_3M_9GN_2$-PP-Dol relative to M_9GN_2-PP-Dol. To obtain some insight into this discrepancy, the yeast OST was assayed using an OS-PP-Dol sample that was obtained by mixing roughly equal concentrations of $G_3M_9GN_2$-PP-Dol (950 nM final) and M_9GN_2-PP-Dol (810 nM final). ^{125}I-labeled glycopeptide products that were collected after 30, 60 or 90 min of incubation were subjected to analytical HPLC using an aminopropyl silica column (*33*) to resolve $G_3M_9GN_2$-NYT from M_9GN_2-NYT. Since the two OS-PP-Dol preparations are relatively homogeneous with respect to oligosaccharide size (85−95%), we can compare the transfer rates for the fully assembled donor ($G_3M_9GN_2$-PP-Dol) and an assembly intermediate (M_9GN_2-PP-Dol) by quantifying all products (M_8GN_2-NYT to $G_3M_9GN_2$-NYT) in the HPLC elution profile (not shown). In this experiment, the normalized transfer rate for the fully assembled donor was 5-fold higher than the transfer rate for M_9GN_2-PP-Dol. This observation, which is in accord with the previous reports cited above, prompted a more thorough analysis of the competition between the two donor substrates.

To investigate how the oligosaccharyltransferase selects $G_3M_9GN_2$-PP-Dol from a mixture of OS-PP-Dol compounds, a donor substrate saturation curve for $G_3M_9GN_2$-PP-Dol was obtained in the presence of a constant saturating concentration (940 nM) of M_9GN_2-PP-Dol. The glycopeptide products, containing M_9GN_2-NYT and $G_3M_9GN_2$-NYT as the major products, were separated by HPLC to allow the calculation of glycopeptide formation rates for both substrates (Figure 6B). The transfer rates for the $G_3M_9GN_2$-PP-Dol donor were slightly reduced relative to the control assays that lacked the competing substrate (compare Figures 5B and 6B). As the concentration of the $G_3M_9GN_2$-PP-Dol donor increased, the transfer rate for the M_9GN_2-PP-Dol donor was substantially reduced (Figure 6B). Lineweaver-Burk plots for $G_3M_9GN_2$-NYT formation did not show the upward curvature that was observed in the absence of the competing substrate (not shown). These observations suggested that the two donor substrates compete for binding to the activator and catalytic sites as depicted in the scheme shown in Figure 6A. The equilibria in Figure 6A shows the possible reaction pathways that would yield a glycopeptide product when two donor substrates ($G_3M_9GN_2$-PP-Dol and M_9GN_2-PP-Dol) compete for ordered binding to the activator and catalytic sites of a substrate-activated bireactant enzyme. In addition to the homotropic interactions that occur between the activator and catalytic sites when both occupied by either $G_3M_9GN_2$-PP-Dol or M_9GN_2-PP-Dol, two heterotropic interactions were also considered. Cooperative heterotropic interactions between the activator and catalytic sites are described by the parameters β (M9RCG3) and γ (G3RCM9).

The steady-state rate equations (see Materials and Methods, eqs 2−5) that were derived for this model were used to fit the experimental data. Due to the large number of variables in the equations, curve fitting was restricted to the two interaction constants (β and γ) for which values had not been obtained in the preceding experiments (Figure 5). Since the k_{cat} value for the enzyme (V_{G3G3} and V_{M9M9}) was not noticeably affected by the structure of the donor substrate, the experimental data was fit assuming that $V_{G3G3} = V_{M9M9} = V_{G3M9} = V_{M9G3}$. The most satisfactory fits of the experimental data were obtained when the β interaction coefficient was low (0.25−0.3) and the γ interaction coefficient was high (1.8−3.5), with a high γ/β ratio (7−12).

When M_9GN_2-PP-Dol was the variable donor substrate in a competition experiment, we observed that 250 nM $G_3M_9GN_2$-PP-Dol was a very potent inhibitor of M_9GN_2-NYT formation (Figure 6C). In contrast, formation of $G_3M_9GN_2$-NYT decreased by less than 20% when M_9GN_2-PP-Dol was present in a 4-fold molar excess. Lineweaver−Burk plots for $Man_9GlcNAc_2$-NYT formation in the presence of the competing substrate showed a downward curvature near the $1/V$ axis, suggesting that V_{max} would be approached when M_9GN_2-PP-Dol is present in large excess relative to $G_3M_9GN_2$-PP-Dol. Satisfactory fits of the experimental data could be obtained using the steady-state rate equations (eqs 2−5) derived for the model depicted in Figure 6A. The most satisfactory fits of the experimental data were obtained when the β interaction coefficient was low (0.15−0.25) and the γ interaction coefficient was high (1.7−3.5), with a high γ/β ratio (11−14). Thus, the two competition experiments could be fit with very similar, albeit not identical, parameters. A closer examination of the data indicates that the slight discrepancy between the calculated parameters is readily explained by experimental deviations between the two competition experiments.

DISCUSSION

A substrate activation mechanism, proposed here to explain the sigmoidal shape of the saturation curves for the OS-PP-Dol substrate, is a special case of the two-site hypothesis proposed by investigators to explain allosteric enzyme kinetics (for a review see, ref *47*). In principle, a substrate activation mechanism assumes the presence of at least two binding sites for the substrate. The two sites are nonequivalent, and one of the sites is a regulatory or activator site. Substrate binding to the activator site induces a conformational change at the catalytic site that alters the affinity for the substrate.

Several lines of kinetic evidence prompted us to consider a two-site model for OS-PP-Dol binding to the OST.

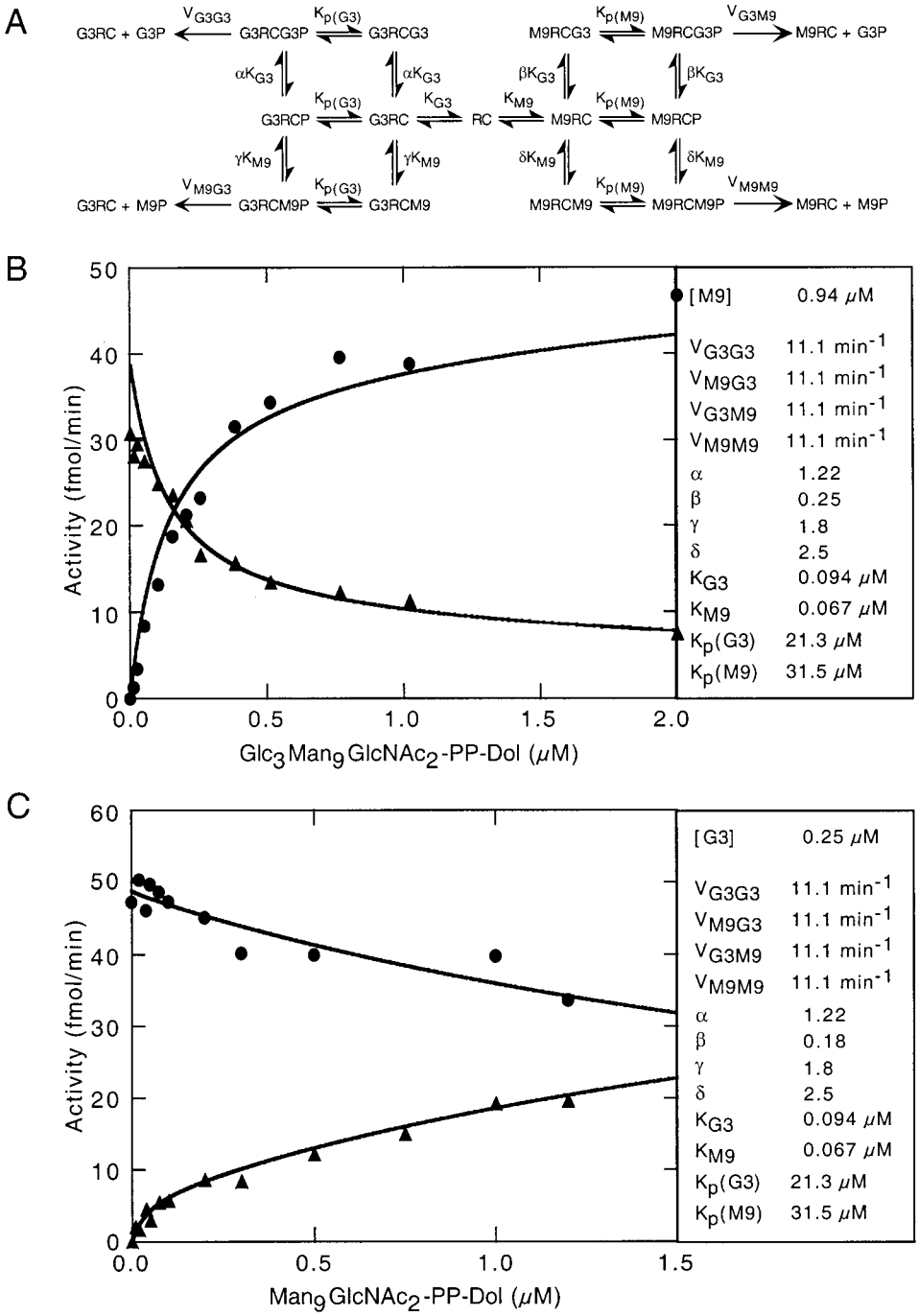

FIGURE 6: Competition between glucosylated and nonglucosylated OS-PP-Dol donor substrates. (A) A kinetic model showing competition between the $G_3M_9GN_2$-PP-Dol (G3) and M_9GN_2-PP-Dol (M9) donor substrates. The reaction equilibria in Figure 5A was expanded to indicate how two different OS-PP-Dol compounds would compete for binding to the R and C sites of the OST. K_{G3} and K_{M9} represent the affinity constants for binding of G3 and M9 to the regulatory site. The interaction factors, α and γ, describe the binding of G3 or M9 to the G3-OST (G3RC) complex, respectively. β and δ are the interaction factors for binding of G3 or M9 to the M9-OST (M9RC) complex. $K_{p(G3)}$ and $K_{p(M9)}$ are affinity constants for binding of peptide to the catalytic site of G3-OST (G3RC) or M9-OST (M9RC) complex. (B and C) OST activity was measured at increasing concentrations of G3 (B) or M9 (C) in the presence of a fixed concentration of either M9 (940 nM) or G3 (250 nM), respectively. The I^{125}-labeled glycopeptide products for each assay point were isolated and analyzed by HPLC. The percentage of $G_3M_9GN_2$-NYT and M_9GN_2-NYT products obtained for each data point was calculated from HPLC profiles and is expressed as enzyme activity (fmol/min). The curves were obtained by fitting the data to eqs 2 and 3 (see Materials and Methods) which were derived from the reaction equilibria shown in panel A. $K_{p(G3)}$ and $K_{p(M9)}$ values were obtained from Figure 2A. The affinity constants (K_{G3} and K_{M9}), the interaction factors (α and δ), and the k_{cat} values (V_{G3G3} and V_{M9M9}) are derived from Figure 5, panels B and C. The β and γ values which gave the most satisfactory fits to the experimental data in panels B and C are shown.

Lineweaver−Burk plots for OS-PP-Dol as the variable substrate showed a pronounced upward curvature. Since the enzyme and the OST are incorporated into liposomes in our assay, the upward curvature cannot be explained by insolubility of the OS-PP-Dol at high concentrations. Enzyme heterogeneity (e.g., K_m or V_{max} differences) is not a plausible explanation, as this would cause downward curvature of a Lineweaver−Burk plot. Second, in the presence of a constant concentration of the alternative donor substrate (e.g., M_9GN_2-PP-Dol), which can bind to either the catalytic or

regulatory sites, the upward curvature of the Lineweaver−Burk plots for the variable donor substrate (e.g., $G_3M_9GN_2$-PP-Dol) was no longer evident. In contrast to the Hill coefficient value of 1 that was observed for the acceptor tripeptide, the Hill coefficients obtained for the donor substrate ranged between 1.33 and 1.4. The simplest interpretation for the latter result is that the enzyme contains a regulatory OS-PP-Dol binding site in addition to a single catalytic site that binds the donor and acceptor substrates. Although the K_s values for the two donor substrates were fairly similar when the donor substrates were assayed separately, the transfer rate for the two donor substrates differed by a factor of 5 when the two substrates were present in a 1:1 molar ratio. This type of behavior strongly suggested that an allosteric activation mechanism was responsible for substrate selection.

According to the substrate activation model depicted in Figure 5, the ability of the OST to discriminate between the glucosylated and nonglucosylated donor substrates is determined by the ratio of two pairs of interaction factors (γ/α and δ/β). Since the affinity of the regulatory site for $G_3M_9GN_2$-PP-Dol and M_9GN_2-PP-Dol is fairly similar (94 and 67 nM, respectively), occupation of the regulatory site will primarily reflect the composition of the donor oligosaccharide pool, which under normal growth conditions will be mainly $G_3M_9GN_2$-PP-Dol. When the regulatory site is occupied by $G_3M_9GN_2$-PP-Dol, the relative affinity of the OST-G3 complex (G3RC) for a second OS-PP-Dol molecule will favor binding of $G_3M_9GN_2$-PP-Dol by roughly 1.5-fold (γ/α) relative to a nonglucosylated donor substrate. Consequently, the OST will primarily transfer the fully assembled donor substrate in vivo both because this compound is the most abundant donor, and because of the homotropic interactions favoring $G_3M_9GN_2$-PP-Dol binding to the catalytic site. However, when the regulatory site is occupied by an assembly intermediate (e.g., M_9GN_2-PP-Dol), the enzyme will display a 10-fold preference (δ/β) for $G_3M_9GN_2$-PP-Dol relative to the assembly intermediates, hence any residual $G_3M_9GN_2$-PP-Dol will be preferentially utilized. Indeed, the initial yeast *alg3* mutant, which is slightly leaky, preferentially utilizes the low amounts of $G_3M_9GN_2$-PP-Dol that are synthesized to glycosylate proteins (*51*).

The substrate activation model can account for the in vivo and in vitro behavior of the OST that has been observed in previous studies when heterogeneous OS-PP-Dol pools serve as the donor substrate. Crude OS-PP-Dol preparations often contain a heterogeneous mixture of OS-PP-Dol compounds ranging between M_3GN_2-PP-Dol and $G_3M_9GN_2$-PP-Dol (*33*), yet the fungal and vertebrate OST will preferentially select $G_3M_9GN_2$-PP-Dol from a complex mixture of donor substrates (*17*). Here, we presented evidence in Figure 1 that the preferential utilization of $G_3M_9GN_2$-PP-Dol observed in the in vitro experiments is not a consequence of detergent solubulization of microsomal membranes. During the early log phase growth of wild-type yeast, approximately 90% of the donor substrate is $G_3M_9GN_2$-PP-Dol, hence this compound is the primary oligosaccharide transferred to nascent glycoproteins. However, as carbon sources in the media are depleted during the late-log phase of growth, the primary donor available is M_9GN_2-PP-Dol which also serves as a substrate for the OST (*50*). Likewise, yeast *alg* mutants that accumulate assembly intermediates (M_5GN_2-PP-Dol to $G_2M_9GN_2$-PP-Dol) synthesize glycoproteins that have relatively modest (<2-fold) reductions in total N-linked oligosaccharides (*25*).

A deviation from Michaelis−Menten enzyme kinetics could also occur upon interaction of two or more OS-PP-Dol binding sites if OST octamers form higher-order oligomers. Several lines of experimental evidence argue against this explanation. Two different epitope-tagged forms of the Stt3p, expressed in a diploid yeast strain, did not coprecipitate under nondenaturing conditions. It has been shown previously that the OST is stable under nondenaturing immunoprecipitation conditions and that all eight subunits, including Stt3p, are present in a 1:1 stoichiometric ratio (*30*). Taken together with earlier hydrodynamic experiments (*32*) estimating a molecular weight of roughly 300K for the enzyme, we conclude that the OST does not form higher-order oligomers that could account for the cooperative OS-PP-Dol binding kinetics.

An alternative explanation for nonhyperbolic OS-PP-Dol saturation kinetics for the donor substrate would be enzyme hysteresis (*48*, *49*). For key regulatory enzymes, a potential physiological benefit of hysteresis is to generate kinetic cooperativity through a slow transition. Other than producing cooperativity, hysteresis can also effect the cooperativity due to site−site interactions in a positive or a negative way. For example, binding of OS-PP-Dol could induce a "slow" conformational change of the enzyme from one form to another with different kinetic properties. Enzyme hysteresis or an enzyme "memory" model does not seem to be likely for the OST due to the linearity of product formation versus time.

We have considered a kinetic model for the OST that assumes a single binding site for both the donor and acceptor substrates, as this would be in accord with the hyperbolic saturation curves for OS-PP-Dol that have been reported by other investigators. According to the reaction scheme shown in Figure 7A, the donor and acceptor substrates bind to the enzyme in a random order, but there is an allosteric interaction between the peptide acceptor and the donor substrate that favors binding of $G_3M_9GN_2$-PP-Dol. An ordered binding mechanism was not considered since the apparent K_m values for the donor and acceptor substrates are not affected by the concentration of the other substrate (Figure 2B). The kinetic parameters (K_{G3}, K_{m9}, V_{G3}, V_{M9}, K_p, a, and b) were obtained by nonlinear least-squares fits of the primary kinetic data displayed in Figures 2, 3, and 5 to eq 6. We then tested this kinetic model by determining whether the competition data shown in Figure 6, panels B and C could be fit to eqs 7 and 8 which were derived according to the equilibria diagram in Figure 7B. As shown in Figure 7, panels C and D, a single-site kinetic scheme for the OST cannot account for the dramatic preference for the fully assembled donor substrate that is observed in the competition experiments.

For many allosteric enzymes, the ligand that binds to the regulatory site is a structurally different molecule than the substrate. In the case described here, the substrate ($G_3M_9GN_2$-PP-Dol) binds to the regulatory site to act as a homotropic activator. More interestingly, a suboptimal substrate analogue (M_9GN_2-PP-Dol) acts as a heterotropic positive activator for $G_3M_9GN_2$-PP-Dol binding and as a

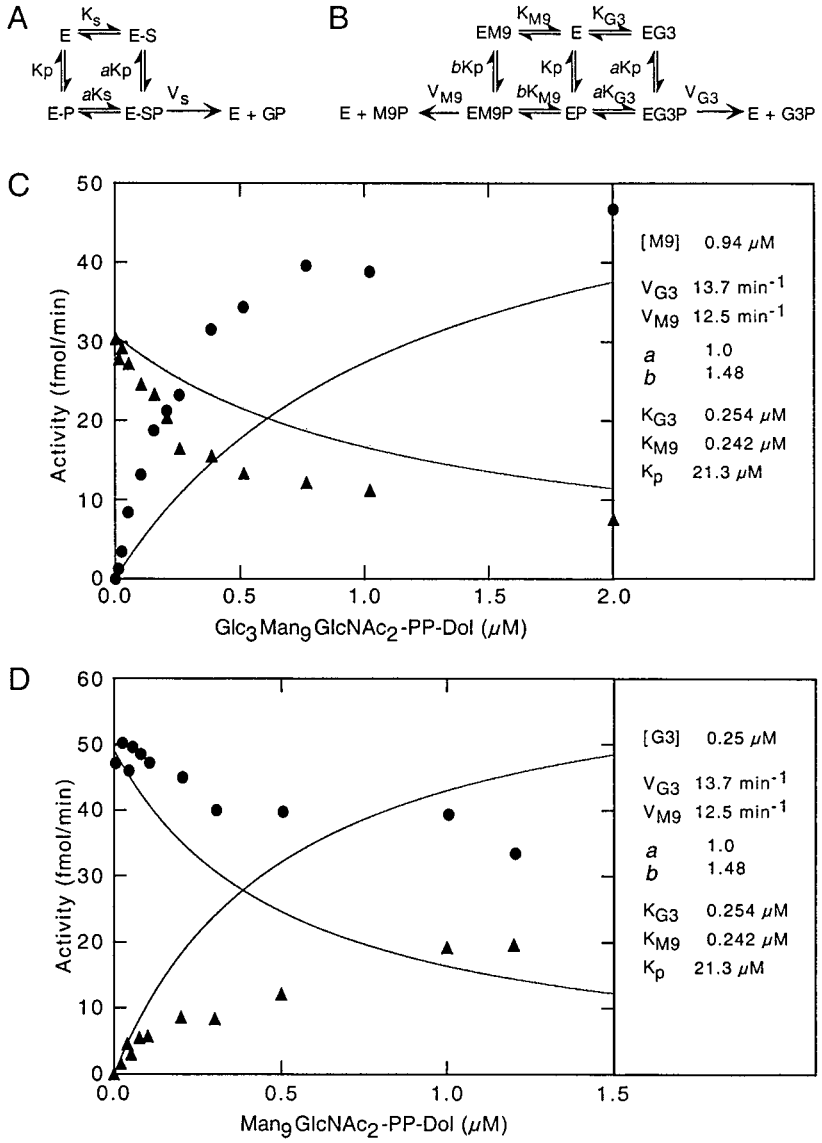

FIGURE 7: Single OS-PP-Dol binding-site model for the OST cannot adequately explain donor substrate competition. (A) A reaction equilibria for a random-order bireactant system with allosteric interaction between the two substrates. (B) A reaction equilibria showing the competition between the G3 and M9 substrates assuming a single binding site for the OS-PP-Dol substrate and a random order of substrate binding. K_p, K_{G3}, and K_{M9} are the affinity constants for random binding of peptide (P), G3, or M9 to the OST (E). The interaction constants (*a* and *b*) describe how the assembly of the enzyme−substrate complex (EPG_3 or EPM_9) is influenced by the structure of the OS-PP-Dol donor. The kinetic parameters were obtained from nonlinear least-squares fit of enzyme activity versus OS-PP-Dol concentration ($G_3M_9GN_2$-PP-Dol or M_9GN_2-PP-Dol) using the steady-state rate equations (7 and 8) derived for the model shown in Figure 7A. Parameters that provided good fits to the experimental data for assays that contained $G_3M_9GN_2$-PP-Dol or M_9GN_2-PP-Dol (not shown) did not yield satisfactory fits when two different donor substrates were combined in the competition experiments (panels C and D).

negative homotropic effector for M_9GN_2-PP-Dol binding to the catalytic site. The physiological importance of a substrate activation mechanism in regulating in vivo enzyme activity has been suggested for other enzymes including phenylalanine hydroxylase, which is activated by phenylalanine (*52*, *53*). A substrate activation model has been proposed for other enzymes to explain kinetic data that yielded nonlinear Lineweaver−Burk plots and could not be fit with the Michaelis−Menten equation. Some of these enzymes, which are proposed to show substrate activation, are also capable of utilizing structurally similar alternative substrates. For example, deoxycytidine kinase exhibits substrate activation with both pyrimidine and purine deoxyribonucleosides, and yet, it has the highest affinity for deoxycytidine as the nucleoside substrate (*54*). For several mammalian liver esterases substrate activation has been observed, and the kinetic results indicate that enzyme specificity depends on the C-chain length of the substrate (*55*).

Although yeast genetic experiments have demonstrated that five (Ost1p, Ost2p, Swp1p, Wbp1p, and Stt3p) of the eight OST subunits are essential gene products (for a review, see ref *2*), the active site has not been localized to a specific yeast OST subunit. Two subunits (ribophorin I and OST48) of the mammalian OST are modified by peptide substrate analogues containing an epoxyethylglycine residue (*56*), suggesting that the respective yeast orthologues (Ost1p and Wbp1p) are candidate subunits for the active site. Likewise, the location of the activator site is uncertain, yet there is evidence that mutations in Stt3p influence donor substrate selection (*57*). Our current data does not allow us to make any predictions about the mechanism of allosteric communication between the activator and the catalytic site, nor

can we predict whether these sites reside on the same or different subunits. It should be pointed out that an obvious structural symmetry is not evident from the primary or theoretical secondary structures of any of the subunits of the OST complex. Localizing distinct and physically nonoverlapping activation and catalytic sites in an enzyme that is proposed to utilize a substrate activation mechanism has not been a trivial task (*58*, *59*). For pyruvate decarboxylase, which is activated by pyruvate, the regulatory information transfer occurs between a pyruvate-bound activation site on the β domain and catalytic sites located between the α and γ domains on different subunits (*58*).

Nonlinear Lineweaver−Burk plots were not observed for the donor substrate in previous kinetic studies of the OST. Several differences in experimental design may account for this discrepancy. Unlike most previous studies, the purified OST and near-homogeneous preparations of the purified donor substrates were used in the experiments described here. Crude enzyme samples prepared from microsomal membranes contain glucosidases I and II that will degrade the donor substrate and glycopeptide product unless glucosidase inhibitors are present. Detergent extracts of microsomes also contain endogenous acceptors and unlabeled donor oligosaccharides that can compete with the radiolabeled assay substrates. The donor oligosaccharide preparations used in the current study have been characterized (*33*) and are 85−95% homogeneous with respect to oligosaccharide composition. Importantly, the M_9GN_2-PP-Dol preparation is devoid of $G_3M_9GN_2$-PP-Dol, so internal competition is not an issue, nor can traces of $G_3M_9GN_2$-PP-Dol account for the observed transfer rates when M_9GN_2-PP-Dol is the donor substrate. OS-PP-Dol preparations that contain heterogeneous mixtures of donor substrates yield misleading kinetic data (Karaoglu, Kelleher, and Gilmore, unpublished results). In this study, an 80-fold concentration range of the donor substrate was tested in the typical kinetic experiment (Figure 5). In previous studies, it was simply not feasible to test a broad OS-PP-Dol concentration range due to the low specific activity of the monosaccharide precursors (e.g., C^{14} glucose or H^3 mannose) used for metabolic labeling of OS-PP-Dol and the radiochemical quantities of the donor substrate that could be isolated (*5*, *6*, *12*). The upward curvature we observed in Lineweaver−Burk plots would be far less apparent if the data points obtained at high and low concentrations of the donor substrate were omitted. It is worth noting that the initial kinetic characterization of several other enzymes that utilize a substrate activation mechanism [e.g., porcine kallikrein (*60*), myosin adenosine triphosphatase (*61*), purine deoxyribonucleoside kinase (*54*)] overlooked the sigmoidal kinetics due to the narrow concentration range of substrate analyzed. Finally, the evaluation of the kinetic data with additional graphical methods (Hill plots, *V* vs [S], etc) provided further evidence in favor of sigmoidal binding kinetics.

Although our findings for the kinetic properties of OS-PP-Dol binding to the OST were quite unanticipated and novel, the linear Lineweaver−Burk plots that were obtained for the tripeptide substrate yielded apparent K_m values that are comparable to the values reported by previous investigators (*5*, *9*, *14*). The donor oligosaccharide-dependent difference in the apparent K_m values for the tripeptide acceptor ($K_{pG3} = 21.3\ \mu M$; $K_{pM9} = 31.5\ \mu M$), albeit slight, was consistently observed in multiple experiments and, therefore, was taken into account in the proposed kinetic model. A donor substrate-induced affinity difference, which has been reported in previous studies (*9*, *15*), contributes to the specificity of the OST toward the fully assembled donor oligosaccharide. It should be noted that the apparent V_{max} of the enzyme, when both substrates are saturating, is not dependent upon the oligosaccharide structure of the donor substrate. This observation is in agreement with a recent kinetic investigation of the OST (*9*). Our results provide the first evidence for allosteric communication between regulatory and catalytic OS-PP-Dol binding sites on the yeast OST complex. The proposed kinetic model for the OST should provide a framework for OS-PP-Dol binding experiments.

ACKNOWLEDGMENT

The authors want to acknowledge helpful discussions with Anthony Carruthers and Duane Jenness.

REFERENCES

1. Herscovics, A., and Orlean, P. (1993) *FASEB J. 7*, 540−550.
2. Silberstein, S., and Gilmore, R. (1996) *FASEB J. 10*, 849−858.
3. Gavel, Y., and Von Heijne, G. (1990) *Protein Eng. 3*, 433−442.
4. Hart, G. W., Brew, K., Grant, G. A., Bradshaw, R. A., and Lennarz, W. J. (1979) *J. Biol. Chem. 254*, 9747−9753.
5. Chalifour, R. J., and Spiro, R. G. (1988) *J. Biol. Chem. 263*, 15673−15680.
6. Sharma, C. B., Lehle, L., and Tanner, W. (1981) *Eur. J. Biochem. 116*, 101−108.
7. Bause, E. (1983) *Biochem. J. 209*, 331−336.
8. Bause, E., Breuer, W., and Peters, S. (1995) *Biochem. J. 312*, 979−985.
9. Gibbs, B. S., and Coward, J. K. (1999) *Bioorg. Med. Chem. 7*, 441−447.
10. Ronin, C., Granier, C., Caseti, C., Bouchilloux, S., and Van Rietschoten, J. (1981) *Eur. J. Biochem. 118*, 159−164.
11. Bause, E. (1984) *Biochem. Soc. Trans. 12*, 514−517.
12. Spiro, M. J., Spiro, R. G., and Bhoryoo, V. D. (1979) *J. Biol. Chem. 254*, 7668−7674.
13. Trimble, R. B., Byrd, J. C., and Maley, F. (1980) *J. Biol. Chem. 255*, 11892−11895.
14. Franc, J.-L., and Bouchilloux, S. (1984) *Biochim. Biophys. Acta 800*, 166−170.
15. Breuer, W., and Bause, E. (1995) *Eur. J. Biochem. 228*, 689−696.
16. Jackson, B. J., Warren, C. D., Bugge, B., and Robbins, P. W. (1989) *Arch. Biochem. Biophys. 272*, 203−209.
17. Bosch, M., Trombetta, S., Engstrom, U., and Parodi, A. J. (1988) *J. Biol. Chem. 263*, 17360−17365.
18. Spiro, R. G. (2000) *J. Biol. Chem. 275*, 35657−35660.
19. Parodi, A. J. (2000) *Annu. Rev. Biochem. 69*, 69−93.
20. Ellgaard, L., Molinari, M., and Helenius, A. (1999) *Science 286*, 1882−1888.
21. Petrescu, A. J., Butters, T. D., Reinkensmeier, G., Petrescu, S., Platt, F. M., Dwek, R. A., and Wormald, M. R. (1997) *EMBO J. 16*, 4302−4310.
22. Huffaker, T. C., and Robbins, P. W. (1983) *Proc. Natl. Acad. Sci. U.S.A. 80*, 7466−7470.
23. Chapman, A., Li, E., and Kornfeld, S. (1979) *J. Biol. Chem. 254*, 10243−10249.
24. Liu, T., Stetson, B., Turco, S. J., Hubbard, S. C., and Robbins, P. W. (1979) *J. Biol. Chem. 254*, 4554−4559.
25. Burda, P., and Aebi, M. (1999) *Biochim. Biophys. Acta 1426*, 239−257.
26. Turco, S. J., Stetson, B., and Robbins, P. W. (1977) *Proc. Natl. Acad. Sci. U.S.A. 74*, 4410−4414.
27. Burda, P., and Aebi, M. (1998) *Glycobiology 8*, 455−462.
28. Sherman, F. (1991) *Methods Enzymol. 194*, 1−21.

29. Sambrook, J., Fritsch, E. F., and Maniatis, T. (1989) *Molecular cloning: A laboratory manual*, 2nd ed.; Cold Spring Harbor Laboratory Press, Plainview, NY.
30. Karaoglu, D., Kelleher, D. J., and Gilmore, R. (1997) *J. Biol. Chem. 272*, 32513−32520.
31. Karaoglu, D., Kelleher, D. J., and Gilmore, R. (1995) *J. Cell Biol. 130*, 567−577.
32. Kelleher, D. J., and Gilmore, R. (1994) *J. Biol. Chem. 269*, 12908−12917.
33. Kelleher, D. J., Karaoglu, D., and Gilmore, R. (2001) *Glycobiology 11*, 321−333.
34. Schagger, H., and von Jagow, G. (1991) *Anal. Biochem. 199*, 223−231.
35. Karaoglu, D., Silberstein, S., Kelleher, D. J., and Gilmore, R. (1995) *C. S. H. S. Q. B. LX*, 83−92.
36. Walter, P., and Blobel, G. (1983) *Methods Enzymol. 96*, 84−93.
37. Segel, I. H. (1975) pp 273−401, Wiley, New York.
38. Spirig, U., Glavas, M., Bodmer, D., Reiss, G., Burda, P., Lippuner, V., te Heesen, S., and Aebi, M. (1997) *Mol. Gen. Genet. 256*, 628−637.
39. Knauer, R., and Lehle, L. (1999) *J. Biol. Chem. 274*, 17249−17256.
40. Kelleher, D. J., Kreibich, G., and Gilmore, R. (1992) *Cell 69*, 55−65.
41. Kumar, V., Heinemann, S., and Ozols, J. (1994) *J. Biol. Chem. 269*, 13451−13457.
42. Kumar, V., Korza, G., Heinemann, F. S., and Ozols, J. (1995) *Arch. Biochem. Biophys. 320*, 217−223.
43. Pathak, R., and Imperiali, B. (1997) *Arch. Biochem. Biophys. 338*, 1−6.
44. Imperiali, B., Shannon, K. L., Unno, M., and Rickert, K. W. (1992) *J. Am. Chem. Soc. 114*, 7944−7945.
45. Imperiali, B., and Hendrickson, T. L. (1995) *Bioorg. Med. Chem. 3*, 1565−1578.
46. te Heesen, S., Lehle, L., Weissman, A., and Aebi, M. (1994) *Eur. J. Biochem. 224*, 71−79.
47. Stadtman, E. R. (1966) *Adv. Enzymol. Relat. Areas Mol. Biol. 28*, 41−154.
48. Ricard, J., and Cornish-Bowden, A. (1987) *Eur. J. Biochem. 166*, 255−272.
49. Neet, K. E., and Ainsle, G. R. (1980) *Methods Enzymol. 64*, 192−226.
50. Trimble, R. B., Maley, F., and Tarentino, A. L. (1980) *J. Biol. Chem. 255*, 10232−10238.
51. Verostek, M. F., Atkinson, P. H., and Trimble, R. B. (1991) *J. Biol. Chem. 266*, 5547−5551.
52. Shiman, R., and Gray, D. W. (1980) *J. Biol. Chem. 255*, 4793−4800.
53. Shiman, R. (1980) *J. Biol. Chem. 255*, 10029−10032.
54. Sarup, J. C., and Fridland, A. (1987) *Biochemistry 26*, 590−597.
55. Hofstee, B. H. J. (1972) *Biochim. Biophys. Acta 258*, 446−454.
56. Bause, E., Wesemann, M., Bartoschek, A., and Breuer, W. (1997) *Biochem. J. 322*, 95−102.
57. Zufferey, R., Knauer, R., Burda, P., Stagljar, I., te Heesen, S., Lehle, L., and Aebi, M. (1995) *EMBO J. 14*, 4949−4960.
58. Baburina, I., Dikdan, G., Guo, F., Tous, G. I., Root, B., and Jordan, F. (1998) *Biochemistry 37*, 1245−1255.
59. Rustin, P., Meyer, C. R., and Wedding, R. T. (1988) *J. Biol. Chem. 263*, 17611−17614.
60. Oliveira, L., Araujo-Viel, M. S., Juliano, L., and Prado, E. S. (1987) *Biochemistry 26*, 5032−5035.
61. Yee, D., Wiedner, H., and Eckstein, F. (1980) *Eur. J. Biochem. 113*, 85−90.

BI0111911